Evolution of Crack-Tip Transformation Zones in Superelastic Nitinol Subjected to In Situ Fatigue: A Fracture Mechanics and Synchrotron X-Ray Micro-Diffraction Analysis

S. W. Robertson, A. Mehta, A. R. Pelton, and R. O. Ritchie

2007

Evolution of crack-tip transformation zones in superelastic Nitinol subjected to in situ fatigue: A fracture mechanics and synchrotron X-ray microdiffraction analysis

S.W. Robertson [a], A. Mehta [b], A.R. Pelton [c], R.O. Ritchie [a,*]

[a] *Department of Materials Science and Engineering, University of California, Berkeley, CA 94720, USA*
[b] *Stanford Synchrotron Radiation Laboratory, Menlo Park, CA 94025, USA*
[c] *Nitinol Devices and Components, Fremont, CA 94539, USA*

Abstract

The ultrahigh spatial resolution ($\sim$1 μm^2) of synchrotron X-ray microdiffraction is combined with fracture mechanics techniques to directly measure in situ three-dimensional strains, phases and crystallographic alignment ahead of a growing fatigue crack (100 cycles in situ) in superelastic Nitinol. The results provide some surprising insights into the growth of cracks in phase-transforming material at the microscale. Specifically, despite a macroscopic superelastic strain recovery of 6–8% associated with the phase transformation, individual austenite grains experience local strains of less than 1.5%. This observation indicates that it is the localized process of the accommodation of the transformation and subsequent loading of the martensite that provide the main source of the large recoverable strains. Furthermore, the plastic region ahead of the crack is composed of deformed martensite. This micromechanical transformation process is dependent upon the material texture, and directly influences the transformation zone size/shape as well as the crack path.
© 2007 Acta Materialia Inc. Published by Elsevier Ltd. All rights reserved.

Keywords: Nitinol; Fatigue; Crack growth; Synchrotron X-rays; Microdiffraction

1. Introduction

Nitinol, a nearly equiatomic alloy of Ni and Ti, has become increasingly important for a variety of applications involving biomedical implants, dentistry, aerospace, structural engineering, and sports and leisure equipment. In particular, the alloy has several characteristics – superelasticity, shape memory, corrosion resistance – that make it particularly favorable for the fabrication of biomedical devices, such as endovascular stents. Such stents are manufactured by precision laser machining of deep-drawn thin-walled tubes and shape set processing to achieve the fully open size [1]. Implantation into peripheral arteries and in vivo opera-

tion subject these devices to cyclic stresses, e.g. from pulsatile fatigue in response to the human cardiac rhythm; this can cause cumulative fatigue damage, leading to device fracture and potentially life-threatening scenarios. Whereas superelastic Nitinol displays the desirable mechanical property of very large recoverable strains ($\sim$6–8%) due to an *in situ* austenite-to-martensite phase transformation, its resistance to the stress-driven growth of fatigue cracks is exceptionally low for a metallic material. Despite this, there have been few studies in the literature on this topic [2–10], and none that have focused on developing an understanding at the micron scale and below of how cracks propagate in superelastic Nitinol, expressly in the presence of the in situ phase transformation.

In the present study, attention was centered on understanding the specific nature of the complex phase transformation ahead of a growing crack tip in Nitinol. Whereas

---

* Corresponding author. Tel.: +1 510 486 5798; fax: +1 510 643 5792.
E-mail address: RORitchie@lbl.gov (R.O. Ritchie).

other researchers have investigated crack-tip strains and textures via synchrotron radiation with X-ray spot sizes greater than 400 μm^2 (effectively representing a polycrystalline grain-averaging technique) [11–15], the exact size and shape of a crack-tip plastic, or transformation, zone has surprisingly never been characterized at micron-scale resolution (1 μm^2) (representing a grain-by-grain strain/texture quantification), in either an elastic/plastic or phase-transformation-induced superelastic material. Indeed, the techniques employed herein permit the determination of true three-dimensional strain matrices, unlike the grain-averaging techniques [11–15], which permit only two-dimensional strain estimations. Furthermore, whereas synchrotron radiation sources have been used to map strains and phases in superelastic Nitinol specimens to the same, or lower, resolution [16–21], the only experimental studies centered on the materials with a phase transformation ahead of a crack tip have been performed at much coarser scales, by optical microscopy and Moiré interferometry [22,23]. In the present work, X-ray microdiffraction permits a far greater resolution of ~1 μm^2, with the Laue diffraction patterns providing a direct measure of the atomic response to applied mechanical forces. Moreover, this technique provides a unique tool to distinguish among different modes of strain accommodation, such as transformation strain from the elastic loading of the austenite and martensite phase.

2. Experimental procedures

2.1. Material

Nitinol material, with a composition of Ti–50.8 at.% Ni, was received from Nitinol Devices & Components, Inc. (Fremont, CA) in the form of compact-tension (C(T)) specimens machined from thin-walled Nitinol tubing. This tubing, with a wall thickness of ~0.4 mm, similar to that used for manufacture of self-expanding stents, was cut longitudinally, and then unrolled and shape-set flat. The heat treatments required to produce flattened material from the original tube configuration were similar, both in annealing time and temperature, to the commercial shape-setting procedure utilized for stent manufacture [24]. The flattened material was laser machined into a C(T) specimen geometry, conforming to ASTM Standard E 647 [25], such that all fracture mechanics testing could be performed with the same thickness configuration that is typically used for stents. Specimen dimensions were thickness $B \sim 0.4$ mm and width $W \sim 10.8$ mm, with an initial crack size following fatigue pre-cracking of $a \sim 5.4$ mm. Specimens were then annealed at 750 °C for 30 min to grow the grains from approximately 10 nm to 10–25 μm, i.e. to a size where diffraction scans (with a spot size of ~1 μm^2) could result in several diffraction patterns collected per grain to accurately measure austenite grain-by-grain and intergranular variations. The specimen was further aged (475 °C, 3 min) to tune the austenite finish

temperature, A_f, to ~15 °C such that testing at room temperature would have the same relative deviation ($\Delta T \sim 7$ °C) as experienced by a stent in the human body ($A_f \sim 30$ °C, body temperature ~37 °C); this ΔT approach has been shown to provide accurate modeling of mechanical response in Nitinol [26]. Finally, the specimen was electropolished prior to testing to minimize surface discontinuities and residual stresses from processing, and to produce a stent-like chemically resistant finish.

2.2. Experimental setup

To measure the local strains at a crack tip, a technique was developed that combines micromechanical loading of fracture mechanics specimens with in situ high-resolution imaging via X-ray microdiffraction (at beamline 7.3.3 at the advanced light source synchrotron radiation facility, Berkeley, CA). The C(T) specimen was fatigue pre-cracked ex situ at near-threshold stress intensities[1] ($\Delta K \sim 3$ MPa$\sqrt{m}$, with $K_{max} < 4$ MPa$\sqrt{m}$) to generate an atomically sharp crack with minimal residual stress, using an automated servo-hydraulic MTS mechanical testing system. The pre-cracked specimen was then loaded on the beamline with a custom-designed in situ microtensile loading device [21] to the desired cyclic mode I stress intensity (7.5–15 MPa$\sqrt{m}$, resulting in load ratio,[2] R, of 0.5). In situ fatigue loads were applied in displacement-control with a stepper motor traversing at 0.25 μm s^{-1} and a force capacity of 100 N.

The beamline's microdiffractometer (45 mm sample-to-detector distance) was used to obtain white-beam (5–14 keV) Laue diffraction patterns from very highly localized regions (spot size ~1 μm^2) in the vicinity of the crack tip. Microscopic platinum markers were deposited onto the sample by focused ion beam machining (FIB) to precisely locate and track the crack tip on the diffractometer using X-ray fluorescence. By comparing Laue patterns taken in unstrained material, the local grain orientations, three-dimensional strains and phases were computed at the growing crack tip by analyzing the deviations in the spot locations in diffraction patterns collected near the highly strained crack-tip region; the well-established mathematical algorithms used to compute strain and orientation matrixes from the Laue patterns are described in great detail in Refs. [28,29]. The depth of beam penetration into the C(T) specimen was less than 10 μm (2.5% of the sample thickness), so that plane-stress conditions prevailed. Each contour plot presented herein represents data obtained

---

[1] The stress intensity, K, characterizes the stress and displacement fields in the vicinity of a crack-tip. Here, it is calculated from the relationship: $K = (P_{ap}/BW^{1/2})f(a/W)$, where P_{ap} is the applied load, B and W are, respectively, the sample thickness and width, as defined in Fig. 1, and $f(a/W)$ is a geometric factor of the order of unity [27].
[2] The load ratio, R, is defined as the ratio of the minimum to maximum loads (P_{min}/P_{max}), and hence for tensile loading, it is the ratio of the minimum to maximum stress intensities (K_{min}/K_{max}).

from the analysis of literally thousands of such Laue diffraction patterns collected in a grid pattern around the crack tip, involving hundreds of hours of diffraction pattern collection, several tens of gigabytes of data and days of computational analysis. It should be noted that a total of four C(T) specimens were evaluated using these techniques, with the results herein representing the representative data from just one of those specimens.

3. Results

3.1. Macro scan region (far from the crack tip – fatigue cycle 1)

A large region (~ 1 mm^2) surrounding a crack tip was examined during the first fatigue loading cycle with diffraction collection points spaced on a 16 μm × 16 μm grid that provided a coarse view of the microscopic strains (Fig. 1). Loads were applied in a sequence such that the sample experienced a mode I stress intensity of 7.5 MPa$\sqrt{\mathrm{m}}$ (just below the crack-initiation fracture toughness of 10 MPa$\sqrt{\mathrm{m}}$ [8,10]), followed by continued loading to 15 MPa$\sqrt{\mathrm{m}}$ (close to the onset of catastrophic fracture) and finally reverse loading back to 7.5 MPa$\sqrt{\mathrm{m}}$. The strains presented in Fig. 1 are on the scale of ±1%, which represents the approximate value of the global tensile strain required to induce the austenite-to-martensite phase transformation.

As expected, the largest normal strains occur in the plane of the crack surface in the direction of applied load-ing (the Y direction). Loading to the maximum stress intensity (15 MPa$\sqrt{\mathrm{m}}$) resulted in a dramatic increase in the size and extent of the strains around the crack tip. Reverse loading back to 7.5 MPa$\sqrt{\mathrm{m}}$ naturally resulted in their decrease, although the magnitude of the strains after unloading are much larger than after initial loading to the same stress intensity; this is indicative that cycles of loading can impart residual strains in the vicinity of the crack tip. Although this phenomenon is well known for the cyclic loading of fatigue cracks in traditional elastic–plastic metals, where dislocation plasticity can leave a zone of compressive strain directly ahead of the crack tip (the cyclic plastic zone), it had been uncertain whether similar notions apply to a superelastic material where deformation is accommodated by a totally different mechanism, i.e. via a shear-based phase transformation.

3.2. Local scan region (near the crack tip – fatigue cycles 1–100)

The evolution of strain and microstructure in response to applied low-cycle fatigue (1–100 cycles) was investigated in situ across a highly localized region (180 × 180 μm^2) surrounding a crack tip. The diffraction collection points were spaced on a 3 μm × 3 μm grid with 1 μm^2 spot size, which provided a grain-by-grain resolution of the strains, phases and crystallographic orientations. Fig. 2 shows the local strain and crystallographic alignment (texture) at unloading cycles 1, 2, 10 and 100. The austenite phase was indexed and color-coded according to its associated strain and crys-
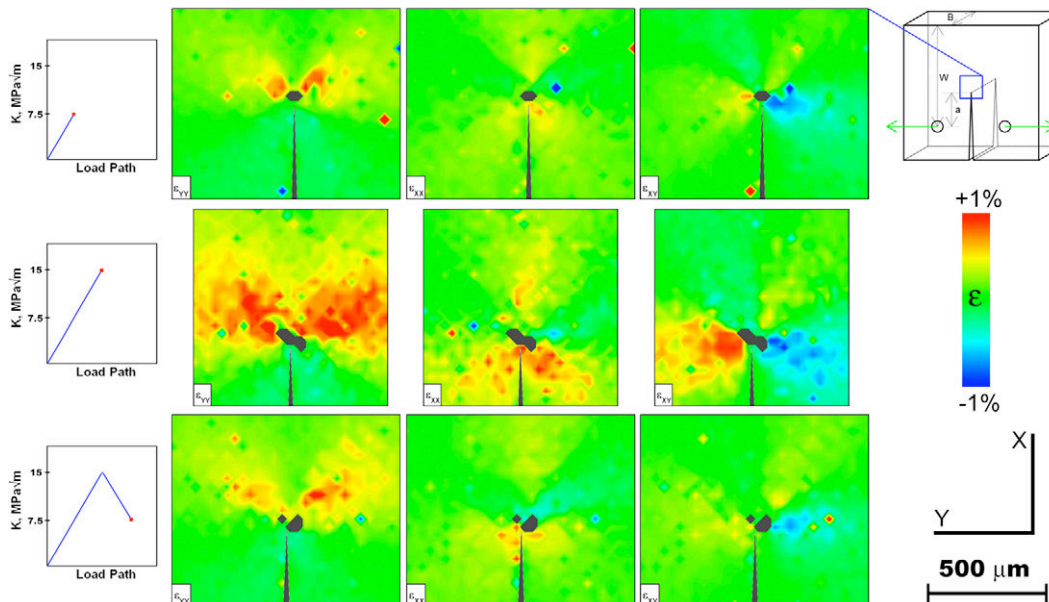

Fig. 1. Strain maps from an ~ 1 mm × 1 mm (16 μm step size) box around the crack tip for the first load/unload fatigue cycle. The top row shows the resultant strains ($\varepsilon_{yy}, \varepsilon_{xx}, \varepsilon_{xy}$) and regions of transformed martensite surrounding a crack loaded from 0 to 7.5 MPa$\sqrt{\mathrm{m}}$, with the black regions representing the crack and the phase-transformed material as determined by an absence of Laue diffraction spots. The second row of contour maps shows a dramatic increase in strains and volume fraction of martensite after the crack was further loaded to a stress intensity of 15 MPa$\sqrt{\mathrm{m}}$. Finally, the sample was reverse loaded back to 7.5 MPa$\sqrt{\mathrm{m}}$, where it is apparent that both the residual tensile strains parallel to the crack face (ε_{yy}) and the martensite volume fraction are much larger than during the first forward cycle of loading. As expected, strains parallel to the loading axis (ε_{yy}) were the greatest, but no far-field strains exceeded ±1%, which is the approximate strain required for the austenite-to-martensite phase transformation in this material.
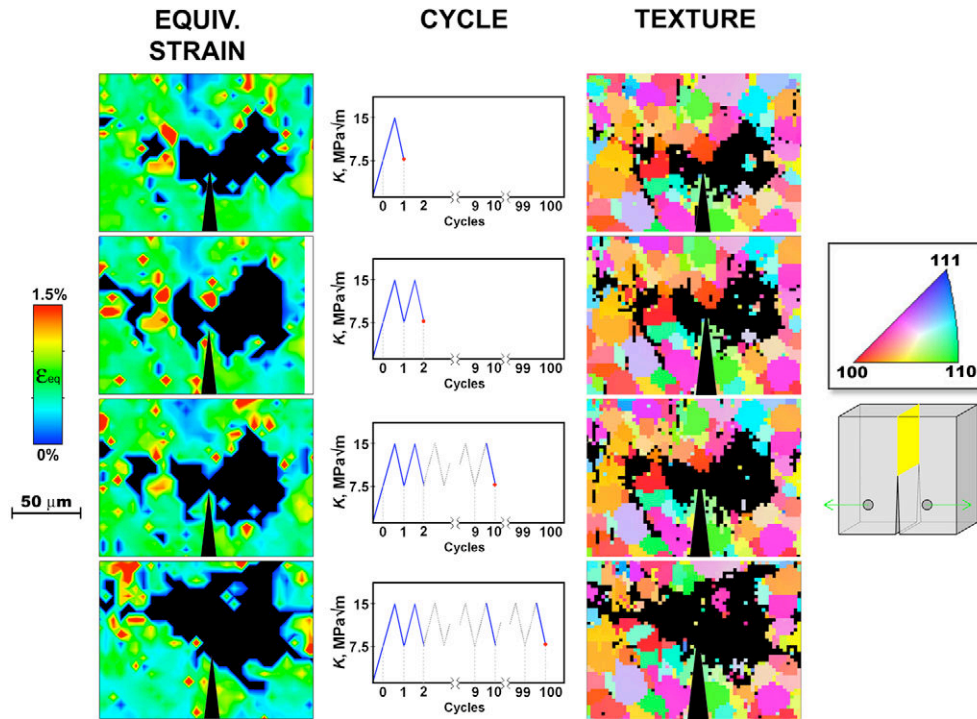
Fig. 2. Local equivalent strain maps, i.e. the combined contribution of the three-dimensional strain matrix per Eq. (1), and grain orientation (texture) maps from fatigue unloading cycles 1, 2, 10 and 100 (each at $K = 7.5 \, \mathrm{MPa}\sqrt{\mathrm{m}}$) showing the evolution of the transformation zone. Strains in the austenite grains surrounding the crack tip were generally in the 0.5–1.0% range (green), with very few grains experiencing strains as high as 1.5%. Texture maps show the grain's planar texture parallel to the crack surface, and demonstrate local anisotropic orientation that influences the direction of the growing fatigue crack.

tallographic alignment (Miller Index). In contrast, the transformed martensite has a nanocrystalline lath structure that is significantly smaller than the incident X-ray beam size; consequently, the white-beam diffraction conditions did not produce any diffraction spots, and martensite is shown as black-colored regions in Fig. 2.

Interestingly, both the equivalent strain maps and grain orientations in Fig. 2 clearly show that material in the wake of the growing crack is predominantly austenite. This indicates that even during catastrophic fracture, the material in the crack wake fully transforms back to the austenite phase on unloading. Moreover, this observation indicates that all structural characterizations of the crack-tip transformation region must be performed under in situ loading in order to derive an accurate picture of the mechanisms of crack propagation in transforming Nitinol.

The size and shape of the forward-advancing transformation zone remains relatively constant between cycles 1 and 10, but appears slightly larger and more diffuse at cycle 100. This is most likely due to interaction of the propagating crack with locally anisotropic grains (i.e. crystallographic orientation differences) as it advances forward. Note that during the 100 fatigue cycles the crack advanced ~30 μm, commensurate with approximately 1 grain.

3.2.1. Crack-tip strain

Equivalent strains surrounding the crack tip were calculated from the three-dimensional strains that were deter-

mined from the Laue diffraction pattern analyses using the relationship [30]:

$$\varepsilon = -\frac{3}{(1+\upsilon)}[\upsilon(\varepsilon'_{xx} + \varepsilon'_{yy}) + (1-\upsilon)\varepsilon'_{zz}], \quad (1)$$

where ε'_{ii} are the deviatoric strains calculated from the Laue diffraction patterns and υ is Poisson's ratio, taken to be 0.33 [31]. A significant finding in this research is that our measurements reveal that the majority of the austenite grains were subjected to only 0.5–1.0% elastic strain (green on the strain scale in Fig. 2). Furthermore, the maximum elastic strain experienced by any austenite grain was only 1.5%, which is near or just above the global threshold for phase transformation (i.e. the onset of the stress plateau in a stress–strain curve), and this was observed for grains only in the region of highest stress/strain within the transformed region.

3.2.2. Crack-tip grain orientations

The grain orientation maps in Fig. 2 show the presence of untransformed grains (~10–25 μm in size) of austenite near the crack-tip (left, and ahead of the crack tips in Fig. 2) that are surrounded by martensite. The two grains that suppress the transformation, the red and green ones in Fig. 2, were oriented with, respectively, their (1 0 0) and (1 1 0) crystallographic faces parallel to the crack surface. The presence of untransformed grains within a zone of sufficient transformation strain suggests that the critical trans-
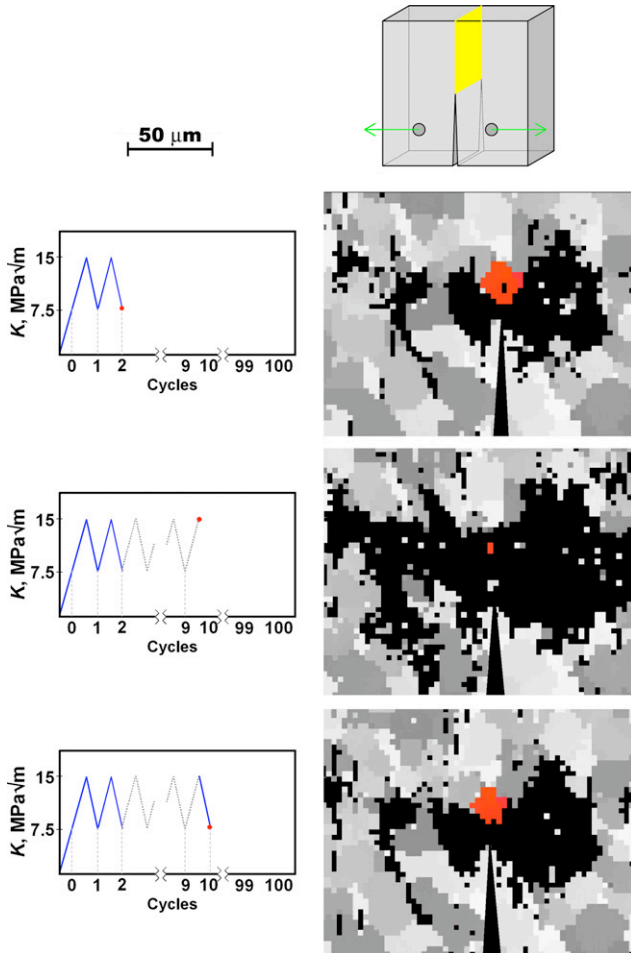
Fig. 3. Evolution of a (100)-oriented grain immediately ahead of the growing crack tip in superelastic austenitic Nitinol which underwent transformation to martensite at K_{max} (15 MPa$\sqrt{m}$), but returned to its same orientation upon unloading to K_{min} (7.5 MPa$\sqrt{m}$).

formation stress has a very large crystallographic anisotropy and the grain alignment (texture) plays a crucial role in the transformation zone and the renormalized stress field ahead of a growing crack tip. From the limited numbers of grain orientations available for observation in a C(T) sample, we were unable to derive a quantitative dependence of the critical stress anisotropy. We have therefore undertaken a companion study on a simpler stress–strain geometry to investigate the mechanism of transformation from austenite to martensite at a local scale in much more detail.[3] It was clear, however, from these texture evaluations that the grains do not reorient as a result of the transformation. This point is made clear in Fig. 3, which shows a (100)-oriented grain immediately ahead of the crack tip which is austenite at $K = 7.5$ MPa$\sqrt{m}$, transforms to martensite at $K = 15$ MPa$\sqrt{m}$ and then returns to its identical (100) ori-

---

[3] For a complete crystallographic description, two planes and one direction need to be specified. Such data were calculated, but, because no clear trends were observed, the orientation results for the extra plane and direction are not included herein.
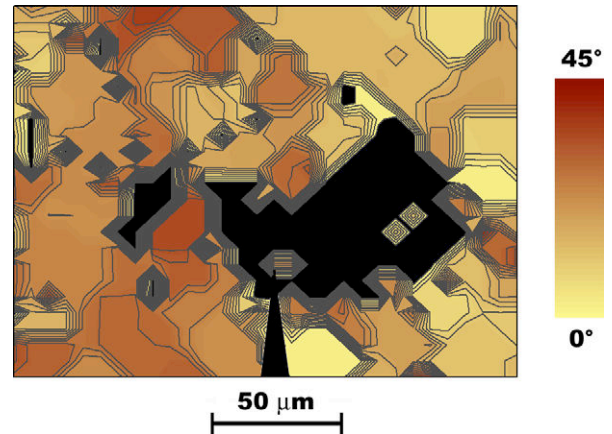

Fig. 4. Lattice misorientation map at $K = 7.5$ MPa$\sqrt{m}$ (first cycle), showing martensitic regions in black and austenite regions in yellow-to-burgundy. Note the presence of subgrain low-angle boundaries within the large-angle grain boundaries. Many of these smaller subgrains transformed to martensite well away from the primary transformation zone, effectively creating a region of mixed phase.

entation upon unloading back to a stress intensity of 7.5 MPa$\sqrt{m}$.

Additional insight may also be gained from Fig. 4, which shows the effect of austenite grain misorientation on the shear transformation in the vicinity of the crack tip (cf. Fig. 1 at 15 MPa$\sqrt{m}$). Clearly there are subgrain boundaries, demarked by low-angle misorientations ($<2°$), contained within the larger grains that are misoriented by more than $10°$ (i.e. high-angle grain boundaries). The fully martensitic transformation zone (shown in black) encompassed several grains immediately surrounding the crack tip. Furthermore, several smaller grains or subgrains beyond the primary transformation zone also transformed to martensite.
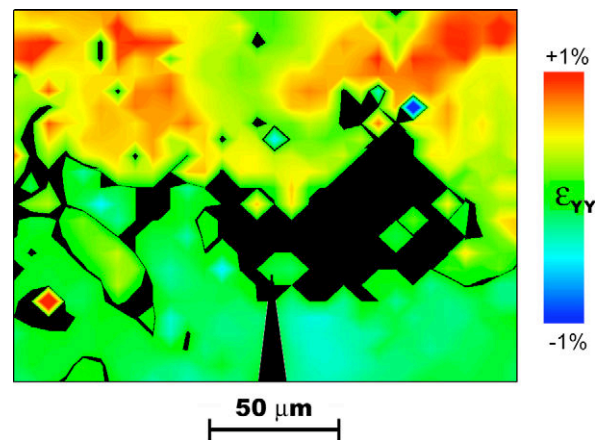

Fig. 5. Austenite strain (ε_{yy}) map at $K = 7.5$ MPa$\sqrt{m}$ showing transformed martensite regions in black (cf. Fig. 4). The austenite tensile strain values range from $+1\%$ (red) to -1% (blue) across this area. Of particular interest are the compressive regions directly ahead and in the wake of the martensite in line with the crack tip. Peripheral areas also show either compressive regions within the tensile zone (upper right) or tensile regions in compressive zones (lower left).

3.2.3. Crack-tip micromechanics

The micromechanics at the propagating crack front is critically affected by the process of transformation from austenite to martensite, which in turn is strongly affected by the local crystallographic orientation of austenite grains, as shown by the untransformed grains within the expected transformation zone in Fig. 2. The high-resolution ε_{yy} strain map at $K_{\min}$ is illustrated in Fig. 5. This figure clearly shows austenite regions that have compressive strains where tensile strains are expected; for example, see the compressive regions on the right above the transformed martensite, and to the left of the crack tip where one would expect full transformation. Furthermore, two regions on the perimeter of the transformation front (right and above, and left and below) demonstrate highly tensile strained austenite islands surrounded by transformed martensite.

4. Discussion

In situ synchrotron X-ray microdiffraction is clearly an unparalleled technique to examine local strains and dynamic phase transformation at a growing crack tip under load in superelastic Nitinol. Although there were many interesting observations made in the course of this investigation, we will concentrate our discussion on the following salient features:

- the effect of austenite–martensite transformation on micromechanics of crack propagation;
- the effect of crystallographic orientation of the austenite size and shape of the transformed martensite region ahead of the advancing crack tip; and
- the effect of stress cycling on the magnitude and distribution of elastic strains in austenite.

4.1. Effects of the martensitic transformation

The size and shape of the transformation zone may be considered by drawing comparisons to the plastic zone size, as estimated from linear-elastic fracture mechanics (LEFM) using isotropic homogeneous yield criteria.[4] It is clear that such a simple LEFM approach has very real limitations in predicting the transformation distributions around a crack tip in an in situ transforming material, specifically since transforming Nitinol (i) displays an anisotropic mechanical response (e.g. Young's modulus of the austenite is twice that of the martensite, $E_a \sim 2E_m$) and (ii) shows texture-specific transformation and hence mechanical anisotropy. The inadequacy of direct application of LEFM to transforming Nitinol has been noted in recent publications [32,33]. Despite these limitations, however, a Nitinol-specific anisotropic yield criterion [32] based

upon the tension–compression asymmetry can be employed to accurately predict the "peanut" shape of the transformation zone. At first glance, this might not seem significant since this shape is well established in plane-strain conditions; however, present samples were under plane-*stress* conditions, such that the "peanut"-shaped zone (with little transformation directly ahead of the crack tip) would not be anticipated when a isotropic homogeneous yield criterion is used.[5]

As such, the present work illustrates that even the modified-LEFM models fail to capture the complex features that are revealed by high-resolution strain analysis. In particular, continuum-based mechanics analyses do not fully reflect the essential and crucial role that the stress-induced phase transformation plays in fracture mechanics of Nitinol and how it alters the understanding of the fracture toughness. As such, it is useful to review the salient features of stress-induced martensitic transformations and then relate these features to the more complex stress fields associated with an advancing crack. Fig. 6a illustrates the applied stress–global strain diagram for transforming Nitinol, i.e. above the A_f (austenite finish) temperature. A key characteristic of stress-induced martensite under these ideal conditions is that the transformation occurs at a single value of applied stress, i.e. the stress plateau is perfectly flat (although in practice there are non-equilibrium effects related to the nucleation of the martensite that give rise to a small stress range). The martensitic transformation also has a very strong crystallographic dependence (as discussed in the next section), and this texture dependence therefore has an impact on the size and shape of the transformation zone; these crystallographic effects are discussed in more detail in a companion paper [34]. Although ∼8% global strain may be accommodated by a combination of elastic, plastic and transformational strain in a region of two-phase mixture of austenite and martensite, this mixed-phase region is stable under a very narrow stress range. Therefore, in a stress-gradient-dominated geometry such as a C(T) specimen, the two-phase region is vanishingly small; and therefore the transition from austenite to martensite must be very abrupt and the two-phase region is very limited, as seen in the strain and grain maps (Figs. 1–5).

In contrast, LEFM-based models (e.g. [32,33]) predict progressively decreasing and continuous stress gradients that radiate away from the crack tip. Indeed (nominally), this has what has been observed in each of the other studies that have utilized synchrotron radiation as a means of characterizing crack-tip zones in aluminum [11,13], steels [12,14] and non-transforming Nitinol [15]. However, it is more precarious to apply these same principles to a phase-transforming material to predict the transformation-zone size and shape. Specifically, such an analysis would predict a region

---

[4] Here the plastic-zone size can be simply estimated by relationships of the form $r_y \sim \beta \, (K/\sigma_y)^2$, where σ_y is the yield strength and β takes values typically between 1/6 and 1/2.

[5] To date, even Nitinol-specific anisotropic yield criteria, such as that proposed in Ref. [32], are not successful in predicting the size of this zone, giving estimates that are roughly six times larger than shown in Figs. 2–5.
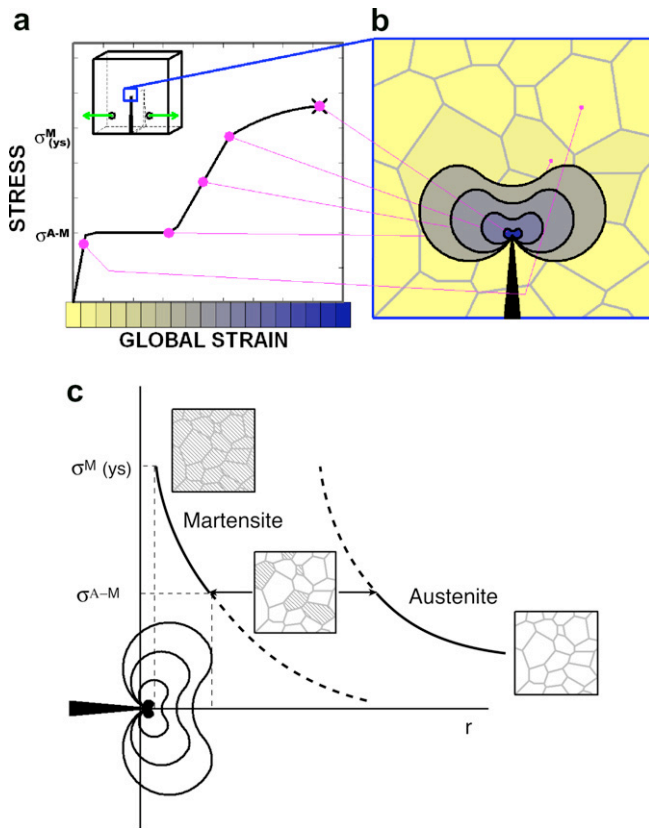
Fig. 6. (a, b) Illustration of the localization of phases as they correlate to a global tensile stress–strain curve. Notice that the transformed zone (corresponding to the black regions in the Figs. 1–3) is comprised of 100% martensite. Experimental results show that grains immediately surrounding this zone are austenite with strains no greater than 1.5%, whereas LEFM would predict a smooth stress gradient. In (c) the distribution of crack-tip stresses according to LEFM is modified to take into account the observations of local compression regions in the austenite that accompany the transformation from austenite to martensite at $\sigma^{\text{A–M}}$. From (a), stress-controlled crack growth implies that above $\sigma^{\text{A–M}}$ there is 100% martensite; (b) shows the approximate shape of the resulting martensite zone.

of fully transformed martensite, surrounded by a continuous mixed-phase region, which in turn is surrounded by 100% austenite. However, this model is contrary to what our data show, and indeed contrary to predictions from thermodynamics of martensitic transformations.

A schematic representation of the phase and local stress distribution surrounding the crack tip is illustrated in Fig. 6b and compared with Fig. 6a. The central core of the transformed region is at the highest stress, and under conditions of K_{max} (close to fracture instability at K_c) this region has locally exceeded the yield stress of martensite shown at the ultimate tensile stress. The successive outer transformed regions depicted in Fig. 6b contain a combination of elastic and plastic stresses in martensite according to the stress–strain diagram. As the local stress drops below the phase-transformation stress, $\sigma^{\text{A–M}}$, martensite is no longer stable and there is a jump to the linear elastic curve of the austenite. The local criteria of significance here is that the crack-tip stress fields must be locally continuous across a transformation boundary. Consequently, when

both the transformation strain ($\sim$4% as discussed in Section 4.2) and elastic moduli mismatch are considered, stress continuity across the interface can be maintained only by locally relieving strain (and sometimes even locally reversing the strain) in both phases. Experimentally, we observe such strain reversals near the crack tip, as shown in Fig. 5. These reversals effectively provide a strain accommodation mechanism with the resultant impact of reducing the local stresses.[6]

It should be noted that the schematic diagram shown in Fig. 6 cannot be directly obtained from the synchrotron X-ray diffraction techniques but rather serves to enhance understanding of the possible stress distributions at the crack tip. Indeed, stress is not an observable quantity at the local state, but can only be inferred from knowledge of local strain and the elastic modulus. As such, in conventional elastic–plastic metals there exists a unique relationship between stress and strain. However, the elastic modulus of NiTi, and therefore the constitutive relationships near the crack-tip, are convoluted by a combination of three primary factors, which have been discussed in previous sections but are summarized here for clarity:

1. There is a contribution from a two-phase mixture, whereby austenite and martensite have distinctly different elastic moduli.
2. The elastic, plastic and transformational strains strongly depend on the local grain orientation.
3. The path dependency of the stress–strain relationship in transforming NiTi (e.g. stress and strain hysteresis) complicates the stress analysis.

Based on the grain and strain maps in Figs. 1–5, we propose a qualitative model, shown in Fig. 6c, for the nominal crack-tip field in the presence of the transformation. Far from the crack tip, there is a subcritical stress in the austenitic grains that follows the linear elastic curve in Fig. 6a. Closer to the crack tip, the critical transformation stress, $\sigma^{\text{A–M}}$, is reached and austenite transforms to martensite. At this stress level, there is an effective jump from the austenite curve to the martensite curve in Fig. 6c. It is appropriate to draw two curves for Nitinol since the phases have such different mechanical properties. The transformation clearly relieves some of the local strain, as shown in Fig. 5, yet in some cases the strain becomes compressive. Consequently, we may draw the martensite curve below that of the austenite; the dotted part of the martensite curve represents a range of stress relief. As such, $\sigma^{\text{A–M}}$ defines the radius of the incipient martensite region and is shown here as the larger boundary. The stresses continue to increase as the tip of the crack is approached and the martensite regions under these higher stresses are depicted with smaller bound-

---

[6] An alternative viewpoint of this phenomenon is that the transformed phase is stable only under an applied force and the energy to stabilize it must come from the local stress field; hence it is a transformation of mechanical energy into internal crystal energy.

aries. The smallest black boundary indicates the size of the plastically deformed martensite, consistent with the "peanut"-shaped region in Fig. 6b. The result of this mechanism is a fully martensite region surrounding the crack tip with strained austenite at the periphery, consistent with the strain and grain maps obtained with this study.

The sharply defined transformed zone in combination with reduction of the stress field at the boundary of the transformed zone has the effect of "renormalizing" the stress field in the vicinity of a crack tip in phase-transforming Nitinol. Consequently, Nitinol should not be thought of as a locally continuous isotropic medium, but rather as a matrix of discrete grains and subgrains that have very different material properties that depend upon their specific crystallographic texture and phase. In this micromechanical view of the fracture mechanics of superelastic Nitinol, crack propagation always occurs in the fully transformed martensite. The mechanical properties of the transformed zone, therefore, are of utmost importance to the fracture mechanics of transforming Nitinol. The stress-induced transformation provides a mechanism of renormalizing the stressed zone. If this renormalization is large, i.e. a large transformation energy, then the resulting reduction in the stress field near a crack can have a beneficial effect of increasing the fracture resistance.

When the crack tip has traversed the martensite region the internal stress field that stabilized the martensite is eliminated and the material transforms back to austenite. This is in contrast to conventional elastic–plastic materials, where the deformed zone at a crack tip can only elastically recover; as such, there are large plastic zones in the wake of the advancing crack. In this respect, superelastic Nitinol is quite different; specifically, there is very minimal residual martensite left in a wake of a propagating crack. For example, a small amount of martensite is seen at the bottom center of Figs. 4 and 5 in the wake of the crack, an effect that we believe is due to the stabilizing effect of plastic deformation of the martensite near the crack tip, whereby the dislocation tangles pin the martensite from transforming back to austenite, as discussed below.

Figs. 1 and 2 also illustrate that there is an increase in the volume fraction of martensite with in situ stress cycling. However, upon one unloading cycle to 7.5 MPa$\sqrt{\text{m}}$, only a portion of the martensite has retransformed to austenite, which again indicates that martensite has been stabilized by local residual elastic strains in austenite as well as plastic strains in martensite. The results from Fig. 2 further illustrate that the volume fraction of martensite continues to increase with increasing number of stress cycles, which may be due to a combination of the orientation of the grains experienced by the advancing crack tip, coupled with the dislocation tangle phenomenon.

4.2. Effects of crystallographic orientation

In Fig. 1 and especially Fig. 2, it is apparent that there is a non-uniform strain distribution in the austenite at stress intensities of both 7.5 and 15 MPa$\sqrt{\text{m}}$, where several austenite grains clearly resist transformation. It is known that both the shape-memory and stress-induced transformation in Nitinol depend on the orientation of the grains. Otsuka et al. [35] described the transformation strain for shape memory in terms of the phenomenological crystallographic theory and noted that these strains are nearly proportional to the Schmid factor used to predict the critical resolved shear stresses for plasticity. Miyazaki et al. [36] found that this theory matched well with the shape-memory transformation strains in $Ti_{49.5}Ni_{50.5}$ single crystals. They found that the maximum transformation strain of ∼10.5% is obtained near $\langle 111 \rangle$, whereas near $\langle 100 \rangle$ the strain is only ∼3%. Robertson et al. [37] studied the crystallographic texture in flattened (polycrystalline) Nitinol tubing used in the current study, and observed a strong $\{221\} \langle 1\bar{2}2 \rangle$ orientation with additional $\langle 111 \rangle$ drawing direction components. They used this preferred texture to calculate the predicted transformation strain as a function of tensile deformation direction based on the Taylor (modified Schmid) factor. Their predictions match well with a maximum transformation strain of between 3.8% and 4.8%, which varied with the angle between the tensile direction and drawing axis. As such, it is reasonable to expect that the orientation of the austenite grains, in combination of the direction of the advancing crack, and the resolved loading direction will strongly influence the tendency of the grains to transform to martensite. However, we have not yet found a clear trend to correlate grain orientation with transformation, possibly because of the imposed complex stress state due to the presence of the crack. A companion paper on the use of synchrotron X-ray diffraction on in situ straining of Nitinol uniaxial tensile specimens will more fully address this topic [34].

4.3. Effect of stress cycling

The strain maps presented in Figs. 1 and 2 clearly differentiate the regions of transformed martensite at the crack tip from the elastically strained austenite in the surrounding regions as a function of applied stress intensity. These strain maps reveal that the cyclic application of stress results in a rather complex microstructure and strain distribution near the crack tip. For example, as expected, the individual strain components (ε_{yy}, ε_{xx} and ε_{xy}) all increase when the stress intensity is increased from 7.5 to 15 MPa$\sqrt{\text{m}}$. Upon unloading back to $K = 7.5$ MPa$\sqrt{\text{m}}$, however, ε_{yy} has larger strain lobes, indicating higher residual tensile strains after only one in situ stress cycle. In contrast, the residual strain components from ε_{xx} and ε_{xy} have not grown to the same extent as ε_{yy} but show some realignment. These observations are unambiguous indications that the stress-induced martensitic transformation in the vicinity of a crack tip has modified the microstructural substructure to a great extent. Nevertheless, it is interesting to note that the austenite reaches a local maximum of about 1.5% strain, although the global strain is considerably

higher at the crack tip. This observation is consistent with an earlier synchrotron-based X-ray diffraction study of superelastic Nitinol subjected to global bending strains up to 6% [21]. It is therefore of considerable interest that, even under triaxial stress states, the maximum austenite strain remains $\leqslant 1.5\%$.

5. Conclusions

Based on a study using synchrotron X-ray microdiffraction, with $\sim 1~\mu m^2$ (i.e. grain-by-grain) spatial resolution, to measure in situ the strains, phases and crystallographic alignment ahead of a growing fatigue crack, subjected to 1–100 cycles between mode I stress intensities of $K_{min} = 7.5~\mathrm{MPa}\sqrt{\mathrm{m}}$ and $K_{max} = 15~\mathrm{MPa}\sqrt{\mathrm{m}}$, in a phase-transforming, superelastic material, austenitic Nitinol, the following conclusions can be made:

1. As anticipated, the three-dimensional calculation of the far-field strains exhibited the maximum strains in the direction of applied load. Those strains were less than 1%, which is nominally commensurate with the tensile transformation strain.
2. The shape of the crack-tip transformation zone and the subsequent fatigue propagation path was clearly influenced by the local texture and consequent micromechanics. Indeed, the transformation front was seemingly affected by the grain orientation (texture) such that certain grains that appeared to be within the transformation zone did not transform. However, crystallographic evaluation over this small region ahead of the crack tip revealed no clear trend in which specific orientations caused the suppression.
3. The transformation-zone shape was consistent with LEFM anisotropic yield criteria demonstrating a region of compression directly ahead of the crack tip (i.e. "peanut" shaped), although the size was significantly overestimated.
4. Forward transformation of individual grains to martensite at K_{max}, and reverse transformation back to austenite at K_{min} did not result in any change in the texture of the austenite grains.
5. Grains in the wake of the crack tip, which correspondingly were unloaded, were seen to transform back to austenite after the crack tip grew some distance away.

Acknowledgements

References

[1] Duerig T, Pelton A, Stockel D. An overview of Nitinol medical applications. Mater Sci Eng A 1999;273–275:149–60.
[2] Melton KN, Mercier O. Fatigue of NiTi thermoelastic martensites. Acta Metall 1979;27:137–44.
[3] Dauskardt RH, Duerig TW, Ritchie RO. Effects of in situ phase transformation on fatigue-crack propagation in titanium–nickel shape-memory alloys. In: Otsuka K, Shimizu K, editors. Shape memory materials. Pittsburgh (PA): MRS International, Materials Research Society; 1989. p. 243–9.
[4] Holtz RL, Sadananda K, Imam MA. Fatigue thresholds of Ni–Ti alloy near the shape memory transition temperature. Int J Fatigue 1999;21(November):S137–45.
[5] McKelvey AL, Ritchie RO. Fatigue-crack propagation in Nitinol, a shape-memory and superelastic endovascular stent material. J Biomed Mater Res A 1999;47(3):301–8.
[6] McKelvey AL, Ritchie RO. Fatigue-crack growth behavior in the superelastic and shape-memory alloy Nitinol. Metall Mater Trans A 2001;32(3A):731–43.
[7] Filip P, Mazanec K. Fatigue behavior of pseudoelastic TiNi thin strips in air and body fluid simulated environments. Kovove Mater-Metall Mater 2003;41(5):300–12.
[8] Robertson SW, Ritchie RO. In vitro fatigue-crack growth and fracture toughness behavior of thin-walled superelastic Nitinol tube for endovascular stents: a basis for defining the effect of crack-like defects. Biomaterials 2007;28:700–9.
[9] Stankiewicz J, Robertson SW, Ritchie RO. On the fatigue-crack growth properties of thin-walled superelastic austenitic Nitinol tube for endovascular stents. J Biomed Mater Res A 2007;81:685–91.
[10] Robertson S, Ritchie RO. A fracture mechanics based approach to fracture control in biomedical devices manufactured from superelastic Nitinol tube. J Biomed Mater Res B; 2007. doi:10.1002/jbm.b.30840.
[11] James MN, Hattingh DG, Hughes DJ, Wei L-W, et al. Synchrotron diffraction investigation of the distribution and influence of residual stresses in fatigue. Fatigue Fract Engng Mater Struct 2004;27:609–22.
[12] Croft M, Zhong Z, Jisrawi N, Zakharchenko I, et al. Strain profiling of fatigue crack overload effects using energy dispersive X-ray diffraction. Int J Fatigue 2005;27:1408–19.
[13] Steuwer A, Edwards L, Pratihar S, Ganguly S, et al. In situ analysis of cracks in structural materials using synchrotron X-ray tomography and diffraction. Nucl Instr Meth Phys Res B 2006;246:217–25.
[14] Marrow TJ, Steuwer A, Mohammed F, Engelberg D, Sarwar M. Measurement of crack bridging stresses in environment-assisted cracking of duplex stainless by synchrotron diffraction. Fatigue Fract Engng Mater Struct 2006;29:464–71.
[15] Daymond MR, Young ML, Almer JD, Dunand DC. Strain and texture evolution during mechanical loading of a crack-tip in martensitic shape-memory NiTi. Acta Mater 2007;55:3929–42.
[16] Paula AS, Canejo JHPG, Mahesh KK, Silva RJC, Fernandes FMB, Martins RMS, et al. Study of the textural evolution in Ti-rich NiTi using synchrotron radiation. Beam interactions with materials and atoms. Synchrotron radiation and materials science – proc E-MRS 2005 symposium O on synchrotron radiation and materials science. Nucl Instr Meth Phys Res B 2006;246(1):206–10.
[17] Schmahl WW, Khalil-Allafi J, Hasse B, Wagner M, Heckmann A, Somsen C. Investigation of the phase evolution in a super-elastic NiTi

shape memory alloy (50.7 at.% Ni) under extensional load with synchrotron radiation. Mater Sci Eng A 2004;378(1–2):81–5.

[18] Kulkov SN, Mironov YP. Martensitic transformation in NiTi investigated by synchrotron X-ray diffraction: accelerators, spectrometers, detectors and associated equipment. Proceeding of the 10th national synchrotron radiation conference. Nucl. Instr. Meth. Phys. Res. A 1995;359(1–2):165–9.

[19] Imbeni V, Mehta A, Robertson SW, Duerig TW, Pelton AR, Ritchie RO. On the mechanical behavior of Nitinol under multiaxial loading conditions and in situ synchrotron X-rays. In: Pelton AR, Duerig T, editors. Proceedings of the intereational conference on shape memory and superelastic technologies; 2003. p. 267–76.

[20] Mehta A, Imbeni V, Ritchie RO, Duerig TW. On the electronic and mechanical instabilities in Ni50.9Ti49.1. Mater Sci Eng A 2004;378:130–7.

[21] Mehta A, Gong X-Y, Imbeni V, Pelton AR, Ritchie RO. Understanding the deformation and fracture of Nitinol using in situ synchrotron X-ray microdiffraction. Adv Mater 2007;19:1183–6.

[22] Loughran GM, Shield TW, Leo PH. Fracture of shape memory CuAlNi single crystals. Int J Solids Struct 2003;40(2):271–94.

[23] Labossiere PE, Perry KE. The effects of notches and grain size on transformations in Nitinol. In: Pelton AR, Duerig T, editors. Proceedings of the international conference on shape memory and superelastic technologies (SMST), 2003; Pacific Grove (CA): SMST; 2003. p. 259–66.

[24] Pelton AR, DiCello J, Miyazaki S. Optimisation of processing and properties of medical-grade Nitinol wire. Min Invas Ther Allied Technol 2000;9:107–18.

[25] American Society of Testing Materials, International, Subcommittee E08.06. Standard test method for measurement of fatigue crack growth rates. ASTM book of standards, vol. 3.01, Standard E 647; 2005.

[26] Pelton AR, Duerig T, Stöckel D. A guide to shape memory and superelasticity in Nitinol medical devices. Min Invas Ther Allied Technol 2004;13:218–21.

[27] Anderson TL. Fracture mechanics: fundamentals and applications. 3rd ed. Boco Raton, FL: CRC Press; 2004.

[28] Valek BC. Ph.D. Dissertation: X-ray microdiffraction studies of mechanical behavior and electromigration in thin film structures. Stanford University, Stanford (CA), 2003.

[29] Tamura N, MacDowell AA, Spolenak R, Valek BC, Bravman JC, Brown WL, et al. Scanning X-ray microdiffraction with submicrometer white beam for stress/strain and orientation mapping in thin films. J Synchrotron Rad 2003;10:137–43.

[30] Robertson SW. Ph.D. Dissertation: On the mechanical properties and microstructure of Nitinol for biomedical stent applications. University of California Berkeley (CA), December 2006.

[31] Belousov OK. Temperature dependence of the physical properties and the relationship of transformation in TiNi with the phase diagram. Russ Metall 1981;2:204–6.

[32] Lexcellent C, Blanc P. Phase transformation yield surface determination for some shape memory alloys. Acta Mater 2004;52: 2317–24.

[33] Freed Y, Banks-Sills L. Crack growth resistance of shape memory alloys by means of a cohesive zone model. J Mech Phys Solids; 2007. doi:10.1016/j.jmps.2007.03.002.

[34] Mehta A, Robertson SW, Barney M, Schroeder V, Mitchell M, Pelton AR, et al. In situ synchrotron X-ray microdiffraction investigation of austenite-to-martensite phase transformations in superelastic Nitinol, unpublished work, 2007.

[35] Otsuka K, Wayman CM, Nakai K, Sakamoto H, Shimizu K. Superelasticity effects and stress-induced martensitic transformations in Cu–Al–Ni alloys. Acta Metall 1976;24:207.

[36] Miyazaki S, Kimura S, Otsuka K, Suzuki Y. The habit plane and transformation strains associated with the martensitic transformation in Ti–Ni single crystals. Scripta Metall 1984;18(9):883–8.

[37] Robertson SW, Gong XY, Ritchie RO. Effect of product form and heat treatment on the crystallographic texture of austenitic Nitinol. J Mater Sci 2006;41:621–30.